

**An energy and enstrophy constrained parameterization of barotropic eddy
potential vorticity fluxes.**

Rosie E. Eaves,^a James R. Maddison,^b David P. Marshall,^b and Stephanie Waterman,^c

^a *Department of Physics, University of Oxford, Oxford, UK.*

^b *School of Mathematics and Maxwell Institute for Mathematical Sciences, The University of
Edinburgh, Edinburgh, UK.*

^c *Department of Earth, Ocean and Atmospheric Sciences, University of British Columbia,
Vancouver, British Columbia, Canada.*

Corresponding author: Rosie Eaves, rosie.eaves@physics.ox.ac.uk

10 ABSTRACT: A parameterization for barotropic eddy potential vorticity fluxes is introduced which
11 applies both an energetic and an enstrophetic constraint to down-gradient PV mixing. An eddy
12 kinetic energy budget and an eddy potential enstrophy budget are employed to constrain the
13 parameterized eddy PV fluxes. The parameterization is tested for freely-decaying turbulence over
14 variable bottom topography. Results of the simulations show that the parameterization can convert
15 energy from the parameterized eddies to the mean flow. Furthermore, the kinetic energy and
16 potential enstrophy budgets employed are sufficient to constrain the large-scale flow such that no
17 spurious source of energy is introduced. As a result, the parameterization is able to produce a
18 topography-following flow of the correct order of magnitude when compared with a high-resolution
19 simulation.

20 SIGNIFICANCE STATEMENT: Small-scale eddies in the ocean, the analogue of atmospheric
21 weather systems, are an important factor in determining the large-scale flow. In particular, in
22 regions where the height of the ocean floor varies, eddies drive the flow towards a structure which
23 resembles that of the ocean floor. Current methods of representing eddies in climate models are
24 unable to capture the latter process because they fail to represent accurately the underlying physical
25 processes that constrain the eddies. Here we present a new method for representing ocean eddies
26 in climate models which uses conservation of energy, and of a similar quantity that measures the
27 amount of turbulent stirring, to constrain the feedback of the eddies on the large-scale flow. We
28 test the new method experimentally in a simple computational ocean model, analysing both the
29 parameters that are important in the underlying physics and the large-scale flows produced by the
30 eddies.

31 1. Introduction

40 Topography-following flows dominate the flow structure in the Arctic Ocean (Nand Isachsen
41 2003), a region which plays a crucial role in the global ocean circulation (Wang et al. 2018) and,
42 as such, is influential in both global and localized climates. Bretherton and Haidvogel (1976)
43 first outlined a mechanism through which turbulence drives the flow to a topography-following
44 state. It is well known that the ocean interior is dominated by geostrophic turbulence, in which
45 kinetic energy is cascaded to large scales while potential enstrophy is cascaded to small scales
46 where it is dissipated. Bretherton and Haidvogel (1976) argued that eddies dissipate potential
47 enstrophy while conserving total energy. Consequently, freely-decaying turbulence tends towards
48 a minimum potential enstrophy state for a given initial energy, in which streamlines follow
49 the topography contours. Crucially, these flows arise as a result of the turbulent cascades and
50 hence they are eddy-driven. Since eddies are parameterized in the majority of CMIP6 models
51 with an ocean component (Eyring et al. 2016; Gregory et al. 2016; Griffies et al. 2009, 2016;
52 Jones et al. 2016), the ability of climate models to simulate eddy-driven topography-following
53 flows is reliant on that of the eddy parameterization employed. Since the theoretical argument
54 for the development of topography-following flows begins with the fact that eddies dissipate
55 potential enstrophy while conserving total energy, it is sensible to suggest that an eddy param-
56 eterization which can produce realistic topography-following flows must also have these properties.

58 One method of parameterizing eddy-driven topography-following flows is the Neptune pa-
 59 rameterization (Holloway 1992). Based on the idea of maximum entropy production, Holloway
 60 (1992) used the cascades of energy and enstrophy inherent to the flow to derive a solution for
 61 the flow field with maximised entropy. The Neptune parameterization relaxes the resolved flow
 62 towards a simplified estimate of this maximum entropy flow field, which follows topographic
 63 contours. Neptune has been implemented and tested in both a global (Eby and Holloway 1994)
 64 and Arctic regional (Nazarenko et al. 1998) model. In both studies, it was found that inclusion
 65 of Neptune led to flow fields which are more in agreement with observations than simulations
 66 without Neptune. For example, the inclusion of the parameterization results in the production of
 67 poleward eastern boundary undercurrents and equatorward western boundary undercurrents (Eby
 68 and Holloway 1994), as well as a more complicated surface and sub-surface flow field including a
 69 cyclonic flow in the Makarov Basin, anticyclonic flow around the Chuchki Plateau, and a returning
 70 flow along the Lomonosov Ridge (Nazarenko et al. 1998). However, Eby and Holloway (1994)
 71 noted that there were instances where the abyssal flow produced by Neptune may have been too
 72 strong, resulting in, for example, a reversed depth-integrated total transport of the California
 73 Current system. These studies highlight how the inclusion of eddy-driven topography-following
 74 flows can lead to a more accurate representation of the large-scale circulation. However,
 75 implementation Neptune in climate models is rare.

77 The prevailing eddy parameterization in CMIP6 models is Gent and McWilliams (1990)
 78 (hereafter referred to as GM90). GM90 parameterizes the eddy-induced transport arising from
 79 the eddy buoyancy fluxes as a prescribed advection of tracers, resulting in an adiabatic flattening
 80 of isopycnals. Through this process, energy is converted from potential energy in the large-scale¹
 81 flow to eddy energy, thus mimicking the effects of baroclinic instability. Physically, this results
 82 in a flattening of isopycnals. Whilst the implementation of GM90 into climate models has led to
 83 many improvements (Danabasoglu et al. 1994), there are some limitations. GM90 assumes flat
 84 topography, resulting in flattened isopycnals regardless of the topographic structure, and hence
 85 leads to an unrealistic state of rest over variable bottom topography (Adcock and Marshall 2000).
 86 Additionally, the eddy energy converted from potential energy by GM90 is lost and no longer

¹In the context of eddy parameterizations, the terms large-scale and eddy are used to signify the resolved and unresolved dynamics respectively.

87 accounted for in the system. In reality, quasi-geostrophic theory predicts that part of this eddy
88 energy should cascade to larger scales (Rhines 1975) and can therefore have a direct impact on the
89 large scale flow. GM90 provides no such mechanism for this to occur and therefore introduces a
90 spurious sink of energy into the system. Hence, GM90 does not conserve energy.

91
92 An alternative method for parameterizing mesoscale ocean eddies is that of potential vor-
93 ticity (PV) mixing, in which the eddy PV fluxes are parameterized as fluxing PV down the
94 mean PV gradient (Green 1970; Marshall 1981). High-resolution numerical experiments have
95 demonstrated that the eddy-induced transport correlates with isopycnic gradients of PV (Marshall
96 et al. 1999), providing an argument for PV mixing over GM90. One advantage of PV mixing as a
97 method of eddy parameterization is that, over variable bottom topography under freely-decaying
98 turbulence, the large scale flow will tend to a topography-following state. To demonstrate why this
99 is true, consider the thought experiment in Figure 1 in which a barotropic fluid layer on an f -plane
100 in the northern hemisphere with a rigid lid lies over a topographic formation. We assume there is
101 no forcing or damping in the domain, i.e. conditions of freely-decaying turbulence. If we assume
102 the initial flow field has no systematic structure in mean relative vorticity, i.e. $\bar{\xi} = 0$ everywhere,
103 then the structure of the mean PV is entirely determined by the spatial structure of depth, H . Thus
104 we have large mean PV over the mount (where H is small), and low mean PV around the mount
105 (where H is large). A down-gradient PV mixing parameterization will flux PV from areas of large
106 mean PV to areas of low mean PV. In this scenario, the only way that mean PV can be conserved
107 following the flow is if $\bar{\xi}$ decreases over the mount and increases around the mount, resulting in the
108 development of a mean circulation along lines of constant depth of topography. However, when
109 κ_{PV} is constant, i.e. an unconstrained PV mixing parameterization, the mean flow will increase in
110 strength until PV is uniform throughout the domain, requiring an increase in energy from that of
111 the initial state. Hence, an unconstrained down-gradient PV mixing parameterization introduces
112 a spurious source of energy into the system and does not conserve energy (Adcock and Marshall
113 2000).

114
115 More recent developments in the design of eddy parameterizations have focused on developing
116 energetically consistent parameterizations via the incorporation of an eddy energy budget.

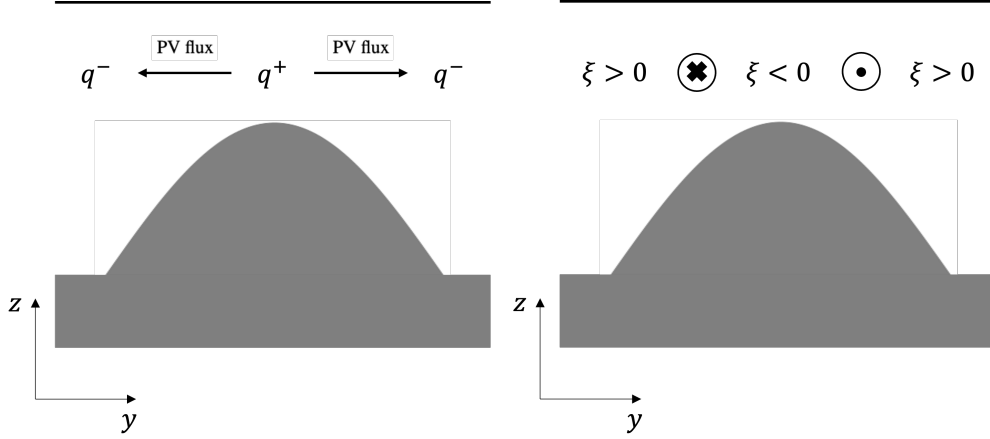


FIG. 1. A thought experiment to demonstrate how down-gradient PV mixing leads to a topography-following flow. Left panel shows the PV flux as a result of a barotropic fluid on an f -plane in the northern hemisphere with a rigid lid lying over a topographic formation and in which there is no systematic structure in the mean relative vorticity, i.e. $\bar{\xi} = 0$ everywhere. In such a case, the PV gradient is determined by the spatial structure of H and a down-gradient PV mixing scheme will act to flux PV from the region over the mount (where PV is large) to the region around the mount (where PV is small). Panel on the right shows the flow as a result of the PV flux indicated in the left panel. Relative vorticity increases in the region around the mount and decreases in the region over the mount, resulting in a circulation along lines of constant topographic depth.

The budget calculates the eddy energy in the system which is then used to inform the eddy parameterization and hence the mean flow. For example, Cessi (2008) and Eden and Greatbatch (2008) incorporated an eddy kinetic energy (EKE) budget into GM90 by combining it with mixing length arguments to determine the eddy diffusivity parameter. Whilst this makes the mean flow energetically consistent with the eddy flow, there is still no mechanism through which EKE can cascade to resolved scales and hence the system is not energy conserving. Bachman (2019) proposed a framework for such a mechanism which re-injects the EKE converted from potential energy by GM90 back into the larger scale barotropic flow via negative diffusion. This results in an improved kinetic energy spectrum at large scales. However, all of these approaches fundamentally rely on using GM90; as a result, they lead to flat isopycnals when implemented over varying topography thus failing to produce a topography-following flow.

Marshall and Adcroft (2010) developed an energetically constrained PV mixing parameter-

130 ization by applying the methods of Eden and Greatbatch (2008) to the PV mixing parameterization
131 framework. By incorporating an energy budget, this approach was able to constrain the
132 effect of the parameterized eddies on the large-scale flow such that it no longer generated a
133 spurious source of energy. Furthermore, they demonstrated that when the eddy PV fluxes
134 are represented as down-gradient PV mixing the growth or decay of the instabilities of the
135 flow was described by a parameterized analogue of Arnold’s first stability theorem (Arnold
136 1965). However, this parameterization was tested in a domain with flat topography and it re-
137 mains to be determined if such a parameterization conserves energy when topography is introduced.

138
139 Another issue related to energy conservation in coarse resolution models is that part of the
140 inverse kinetic energy cascade remains unresolved. This means that kinetic energy at unresolved
141 scales cannot cascade to the larger resolved scales as is typical of geostrophic turbulence. Attempts
142 have been made to parameterize this transfer of energy from unresolved to resolved scales. For
143 example, Jansen and Held (2014) developed such a parameterization which returned the energy
144 dampened at the grid-scale by explicit viscosity back to the resolved flow via a forcing term in the
145 governing equations. The forcing was applied both randomly (using Gaussian noise) and through
146 the use of a negative Laplacian. Mana and Zanna (2014) developed a stochastic parameterization
147 for eddies which represents the effect of the eddies via the divergence of a non-Newtonian stress
148 which was shown to backscatter energy in a wind-driven gyre setup (Zanna et al. 2017). Both
149 studies found that their respective parameterizations led to an improved kinetic energy spectra at
150 all scales (Jansen and Held 2014; Zanna et al. 2017).

151
152 The GEOMETRIC framework (Marshall et al. 2012) is an alternative energetically-constrained
153 parameterization that is based on the decomposition of eddy momentum fluxes into components
154 based on eddy geometry and eddy energy. In the implementation of the GEOMETRIC framework
155 as a parameterization, the eddy energy is solved for prognostically via an energy budget. The
156 geometric parameters, which must be specified, are non-dimensional and strongly bounded in
157 magnitude, making them easier to specify. These parameters also have strong connections with
158 classical stability theory (Marshall et al. 2012; Tamarin et al. 2016). We adopt a similar approach
159 in this study.

160

161 In this paper, we present a new formulation of a barotropic PV mixing parameterization
162 which incorporates an eddy potential enstrophy budget in addition to an EKE budget. The
163 resulting parameterization is therefore both energetically and enstrophetically consistent and the
164 parameterized eddy PV fluxes are constrained by both the eddy potential enstrophy and the EKE.
165 Since the kinetic energy and potential enstrophy cascades are both important factors in the theory
166 underpinning eddy-driven topography-following flows, we hypothesize that incorporating budgets
167 for both will suffice to constrain the down-gradient PV mixing parameterization such that it no
168 longer violates the law of energy conservation when implemented over topography. We test and
169 demonstrate the functionality of the parameterization through a set of highly idealised experiments.

170

171 The rest of this article is structured as follows. In section 2, we outline the formulation of
172 the new energetically- and enstrophetically-constrained down-gradient PV mixing parameteriza-
173 tion. In section 3, we describe our methods related to testing this parameterization in an idealised
174 model, including the experimental design and details about the numerical model set-up. In section
175 4, we compare the results of a barotropic spin-down experiment with random topography at
176 eddy-resolving resolution with that of a coarse resolution simulation in which no parameterization
177 is employed in order to highlight what is required of the parameterization for this problem. In
178 section 5, we present the results of experiments designed to demonstrate the functionality of the
179 parameterization. Finally, in section 6, we summarise and discuss the work presented here as well
180 as avenues for future work.

181 **2. A new parameterization for eddy potential vorticity fluxes**

182 This section outlines a new formulation of a down-gradient PV mixing parameterization as
183 a method for parameterizing the eddy PV fluxes that is both energetically and enstrophetically
184 constrained.

185 *a. Down-gradient potential vorticity mixing parameterizations*

186 Down-gradient PV mixing parameterizations parameterize the eddy PV fluxes as mixing PV
 187 down the mean PV gradient at a specified rate controlled by an eddy diffusivity. This takes the
 188 form

$$\overline{q'\mathbf{u}'} = -\kappa_{\text{PV}} \nabla \overline{q}, \quad (1)$$

189 where \mathbf{u} is the horizontal velocity with components u and v in the zonal (x) and meridional (y)
 190 directions respectively, κ_{PV} is the eddy PV diffusivity, and q is the PV, defined for a barotropic
 191 fluid as

$$q = \frac{f + \xi}{H} \quad (2)$$

192 where f is planetary vorticity, ξ is relative vorticity, defined as $\xi = \partial v / \partial x - \partial u / \partial y$, and H is layer
 193 depth². In Equation (1), and throughout the rest of this paper, overbars denote a time-mean, used
 194 to represent the large-scale, slowly evolving component of the flow, and primes denote a deviation
 195 from the time-mean, used to define the eddy component of the flow.

196 *b. Constraining the eddy potential vorticity fluxes*

197 To constrain the eddy PV fluxes, $\overline{q'\mathbf{u}'}$, we exploit the following bound:

$$|\overline{q'\mathbf{u}'}|^2 \leq 4\Lambda K, \quad (3)$$

198 where Λ is the eddy potential enstrophy and K is the eddy kinetic energy, defined as

$$\Lambda = \frac{\overline{q'^2}}{2}, \quad (4)$$

199 and

$$K = \frac{\overline{u'^2} + \overline{v'^2}}{2}, \quad (5)$$

²Note that H must be invariant with time in order for Equation (1) to be true. In the experiments discussed and analysed in this paper we assume one vertical layer with a rigid lid and a bottom topography that is invariant with time. Hence, this requirement is satisfied.

200 respectively. The bound in Equation 3 holds, for example, for eddy-mean decomposition via time-
 201 averaging as used in this paper. We now employ a similar approach to Marshall et al. (2012) to
 202 construct a down-gradient PV mixing parameterization from Equation (3). An efficiency parameter,
 203 γ_q , can be defined from the bound in Equation (3):

$$|\overline{q'\mathbf{u}'}| = 2\gamma_q\sqrt{\Lambda K}, \quad (6)$$

204 where $0 \leq \gamma_q \leq 1$. Here, γ_q describes how efficient the eddies are at fluxing PV and hence we
 205 refer to it as the PV flux efficiency parameter. When $\gamma_q = 0$, the eddy PV flux is zero on average.
 206 In this case, the eddies do not act to move the system towards a more ordered state. When $\gamma_q = 1$,
 207 the eddy PV flux magnitude is at its maximum value.

208
 209 From the bound in Equation (3), we construct an energetically and enstrophetically con-
 210 strained down-gradient PV mixing parameterization by letting

$$\overline{q'u'} = -2\gamma_q\sqrt{\Lambda K}\cos\phi_q, \quad (7)$$

$$\overline{q'v'} = -2\gamma_q\sqrt{\Lambda K}\sin\phi_q, \quad (8)$$

211 where ϕ_q is the angle of the vector $\nabla\bar{q}$ to the x -axis. This choice for $\overline{q'u'}$ and $\overline{q'v'}$ satisfies the
 212 bound in Equation (3). Since $\nabla\bar{q} = |\nabla\bar{q}|(\cos\phi_q, \sin\phi_q)$, we find that for $\nabla\bar{q} \neq 0$:

$$\overline{q'\mathbf{u}'} = -\frac{2\gamma_q\sqrt{\Lambda K}}{|\nabla\bar{q}|}\nabla\bar{q}. \quad (9)$$

213 Equation (9) describes a down-gradient PV mixing parameterization in which the eddy PV diffu-
 214 sivity is given by

$$\kappa_{\text{PV}} = \frac{2\gamma_q\sqrt{\Lambda K}}{|\nabla\bar{q}|}. \quad (10)$$

215 A key feature of the parameterization is that the magnitude of the eddy PV fluxes are determined
 216 by both the EKE and eddy potential enstrophy in the system. Since κ_{PV} is non-negative, the choice
 217 to include a factor of -1 in Equations (7) and (8) imposes down-gradient PV mixing by design.

One caveat to this approach is that, whilst it is true that the eddies flux PV down the mean PV gradient on average (Marshall and Adcroft 2010), this is not necessarily the case locally (e.g. Waterman and Lilly, 2015). However, imposing down-gradient PV mixing is a common tactic in eddy parameterization design so we deem it a sufficient assumption for this first demonstration-of-concept exercise.

c. Specifying K and Λ

It remains to determine Λ and K , the eddy potential enstrophy and eddy kinetic energy respectively, for use in informing the parameterization. One strategy for determining these parameters is to specify their initial distribution and employ prognostic equations (i.e. an eddy potential enstrophy and EKE budget) to step forward Λ and K at each time step, then using the time-evolving values to inform the parameterization. This strategy ensures that the parameterization is flow-aware. The intention of this formulation is that the parameterization's dependence on time-evolving budgets of Λ and K will act to realistically constrain the energy of the resolved flow.

Following Cessi (2008), Eden and Greatbatch (2008) and Marshall and Adcroft (2010), we employ an EKE budget for a barotropic fluid. The relevant EKE equation is

$$\frac{\partial K}{\partial t} = \overline{q' \mathbf{u}'} \cdot \nabla \bar{\psi} - \frac{1}{H} \nabla \cdot \overline{\mathbf{H} \mathbf{u}' B'} + \mathbf{F}_K, \quad (11)$$

where K is the parameterized EKE, ψ is the transport stream function, B is the Bernoulli potential defined as $B = \mathbf{u} \cdot \mathbf{u} / 2 + p / \rho_0$ where p is the pressure and ρ_0 a reference density, and \mathbf{F}_K represents sources and sinks of eddy kinetic energy.

The first term on the right hand side of Equation (12) represents kinetic energy conversion between the large-scale and eddy components of the flow (Marshall and Adcroft 2010) with a positive value signifying conversion from the mean flow to the eddies. The second term on the right hand side integrates to zero over the domain and therefore acts only to redistribute the energy. Following Eden and Greatbatch (2008) and Marshall and Adcroft (2010), we represent this redistribution of K as advection by the depth-integrated large-scale flow and Laplacian

diffusion with coefficient μ . We include only a sink of K through bottom friction in \mathbf{F}_K which we parameterize as linear drag with coefficient r_K . Thus our EKE budget is

$$\frac{\partial K}{\partial t} = \overline{q'\mathbf{u}'} \cdot \nabla \bar{\psi} - \frac{1}{H} \nabla \cdot (KH\bar{\mathbf{u}}) - r_K K + \mu \nabla^2 K. \quad (12)$$

We also employ an eddy potential enstrophy budget. The relevant eddy potential enstrophy equation is

$$\frac{\partial \Lambda}{\partial t} = -\overline{q'\mathbf{u}'} \cdot \nabla \bar{q} - \frac{1}{H} \nabla \cdot (\Lambda H\bar{\mathbf{u}}) - \frac{1}{H} \nabla \cdot \left(H \frac{\overline{q'^2}}{2} \mathbf{u}' \right) + \mathbf{F}_\Lambda, \quad (13)$$

where Λ is the parameterized eddy potential enstrophy and \mathbf{F}_Λ represents sources and sinks of Λ .

The first term on the right hand side of Equation (14) represents eddy potential enstrophy generation. When $-\overline{q'\mathbf{u}'} \cdot \nabla \bar{q}$ is positive, the eddy PV flux is, on average, down the mean PV-gradient, that is, the eddies act to mix PV. This mixing of PV by the eddies results in a generation of eddy potential enstrophy. When $-\overline{q'\mathbf{u}'} \cdot \nabla \bar{q}$ is negative, the eddy PV flux is, on average, up the mean PV gradient, i.e. the eddies are acting to unmix the PV, resulting in a decrease in the eddy potential enstrophy. Due to the formulation of the parameterization, this term will always be negative in the parameterized simulations and thus acts only to mix PV. The second term on the right hand side represents the advection of eddy potential enstrophy by the depth-integrated large-scale flow. We neglect the third term on the right hand side since it is a product of three eddy terms and is thus assumed to be small. We include both damping of enstrophy at small scales and viscous diffusion in \mathbf{F}_Λ which we represent as linear and Laplacian damping with coefficients r_Λ and μ respectively. Thus our eddy potential enstrophy budget is

$$\frac{\partial \Lambda}{\partial t} = -\overline{q'\mathbf{u}'} \cdot \nabla \bar{q} - \frac{1}{H} \nabla \cdot (\Lambda H\bar{\mathbf{u}}) - r_\Lambda \Lambda + \mu \nabla^2 \Lambda. \quad (14)$$

The energetically and enstrophetically informed down-gradient PV mixing formula, the eddy kinetic energy budget and the eddy potential enstrophy budget (Equations (9), (12) and (14) respectively) describe the parameterization fully. There are four input parameters to the parameterization: the PV flux efficiency parameter, γ_q ; the eddy diffusivity, μ ; the EKE dissipation coefficient, r_K ;

and the eddy potential enstrophy dissipation coefficient, r_Λ . The initial distributions of EKE (K_0) and eddy potential enstrophy (Λ_0) must also be specified. K and Λ evolve with time through their respective budgets and the time-evolving values are then used to determine the magnitude of the down-gradient PV fluxes at each time-step. Employing energy and enstrophy budgets with spatial dependence ensures the parameterization is flow-aware. Through these budgets, the parameterization accounts for the conversion of energy from large-scale to eddy and vice versa, the dissipation of EKE by bottom friction, the generation of enstrophy through PV mixing and enstrophy dissipation at small scales.

It should be noted that Equation (9) does not satisfy the integral constraint necessary for angular momentum in a zonal channel (Marshall 1981; Marshall et al. 2012). We plan to initially test the parameterization in the case of a simply connected basin in which this integral constraint is less of a concern. Further work to satisfy this constraint is left for future work.

3. Methods

a. Experimental design

To analyse the performance of the parameterization, we implement it in an idealised experimental set-up, with which we aim to answer the following key questions:

1. Can the parameterization convert kinetic energy from the eddy field to the large-scale flow, thus producing an eddy-driven topography-following flow?
2. Do the energetics and enstrophics exhibit similar behaviour to their explicit counterparts in an eddy-resolving simulation?
3. How do the input parameters affect the energetics and enstrophics of the dynamics?

To answer these questions, we run a set of numerical simulations in which we simulate barotropic freely-decaying turbulence over random topography on an f -plane. We choose to simulate freely-decaying turbulence over bottom topography since theory predicts that this will lead to an eddy-driven topography-following flow (Bretherton and Haidvogel 1976). We use the following four configurations:

Code	Resolution	Eddies	$\mu_\xi \text{ (m}^{-4}\text{s}^{-1}\text{)}$	γ_q	$r_\Lambda \text{ (s}^{-1}\text{)}$	$r_K \text{ (s}^{-1}\text{)}$	$\mu \text{ (m}^{-2}\text{s}^{-1}\text{)}$	κ_{PV}
5km _{EXP}	5km	Explicit	10^8	-	-	-	-	-
50km _{EXP}	50km	Explicit	10^{11}	-	-	-	-	-
50km _{EECON}	50km	Parameterized	10^{11}	0.1	4.5×10^{-8}	0	500	-
50km _{UNCON}	50km	Parameterized	10^{11}	-	-	-	-	50

TABLE 1. Parameters used in the simulations analysed in Sections 4 and 5.

- (a) an eddy-resolving (5km horizontal resolution) simulation with explicit eddies only (5km_{EXP});
- (b) a coarse-resolution (50km horizontal resolution) simulation with explicit eddies only (50km_{EXP});
- (c) a coarse-resolution simulation with parameterized eddies where we employ an unconstrained down-gradient PV mixing parameterization, i.e. with constant κ_{PV} (50km_{UNCON});
- (d) a coarse-resolution simulation with parameterized eddies as described in Section 2, i.e. with an energetically and enstrophetically constrained down-gradient PV mixing parameterization (50km_{EECON}).

We compare 50km_{EECON} with 50km_{UNCON} to assess if the energetic and enstrophetic constraints imposed are successful in constraining the kinetic energy of the resolved flow. We use 5km_{EXP} as a reference to inform on a realistic kinetic energy for the resolved flow, thus allowing us to determine if the resolved flow is well-constrained by the parameterization. We run many variations of 50km_{EECON} varying the input parameters to the parameterization for each simulation. The details of the simulations are outlined in Table 1.

b. Model equations

In these experiments, we simulate freely-decaying turbulence in a barotropic fluid (i.e. one vertical layer) with a rigid lid. The equations of motion are the mean depth-integrated potential vorticity equation, which, for explicit eddy simulations is

$$\frac{\partial \bar{\xi}}{\partial t} = -\nabla \cdot \bar{\zeta} \bar{\mathbf{u}} - \mu_\xi \nabla^4 \bar{\xi}, \quad (15)$$

and for parameterized eddy simulations is

$$\frac{\partial \bar{\xi}}{\partial t} = -\nabla \cdot \bar{\zeta} \bar{\mathbf{u}} - \nabla \cdot \overline{\zeta' \mathbf{u}'} - \mu_{\xi} \nabla^4 \bar{\xi}, \quad (16)$$

where the eddy PV flux term is replaced with the appropriate parameterization, and the continuity equation,

$$\nabla \cdot \mathbf{H} \bar{\mathbf{u}} = 0, \quad (17)$$

where $\zeta = f + \xi$ and μ_{ξ} is the biharmonic diffusion coefficient. We employ biharmonic diffusion in Equations (15) and (16) for stability.

c. Numerical Implementation

The numerical implementation of time-stepping of Equations 15 and 16 are as follows. The variables are arranged with vorticity, stream function and layer depth defined at the cell vertices. The zonal and meridional components of the velocity are calculated using a centred second-order differencing scheme. We use free-slip lateral boundary conditions, i.e. $\bar{\xi} = 0$ on lateral boundaries, and no flow normal to the boundary, i.e. constant $\bar{\psi}$ on lateral boundaries. For simplicity, we choose $\bar{\psi} = 0$. Advection is calculated using an energy- and enstrophy-conserving scheme defined by Arakawa (1966). Biharmonic diffusion of vorticity is calculated using a centred differencing scheme with $\nabla^2 \bar{\xi} = 0$ on the lateral boundaries.

For parameterized simulations, K and Λ are defined at the cell centre points. We specify a no flux boundary condition for K and Λ , i.e. there is no diffusion or advection of K or Λ through lateral boundaries. Time-stepping of Equations (12), (14), (15) and (16) is computed using the third order Adams-Bashforth method, with the first two time steps calculated using a first-order forward approximation.

d. Specification of Domain Geometry

All simulations are run in a square domain of side length $L = 2000\text{km}$ with non-flat topography. The topography is created by using a seeded pseudorandom number generator (NumPy `random.default_rng`) to generate independent Fourier modes using a Gaussian distribution at 5km

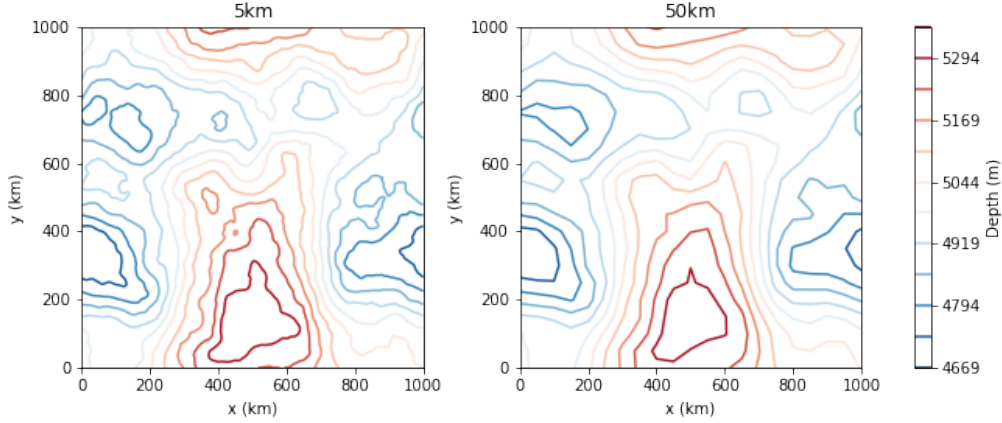


FIG. 2. Topography used in high-resolution simulations (left) and coarse resolution simulations (right).

resolution. A peak wavenumber is specified when generating the Fourier modes to ensure the topography is not confined to small-scale structures. The field generated by the Fourier modes is then multiplied by a constant and translated in depth in order to produce a topography with average depth of 5km and depth variations of around 10%. The topography is regridded using spatial averaging to 50km resolution for the coarse-resolution simulations. The topographic structure used is shown in Figure 2.

e. Specification of Model Parameters

The Coriolis parameter is taken as a constant with value $f_0 = 0.7 \times 10^{-4} \text{ s}^{-1}$ in all simulations. The biharmonic diffusion coefficient, μ_ξ , is set to $10^8 \text{ m}^4 \text{ s}^{-1}$ for simulations at 5km resolution and $10^{11} \text{ m}^4 \text{ s}^{-1}$ for simulations at 50km resolution. These values are chosen to be as small as possible such that grid scale noise is no longer generated. All simulations are run for a total of 3000 days in order to reach a point at which the energy conversion from eddy to mean has plateaued.

For the coarse resolution simulation with the constrained parameterization, 50km_{EECON}, there are four extra parameters for which values need to be specified: the PV flux efficiency parameter, γ_q ; the enstrophy damping parameter, r_Λ ; the energy damping parameter, r_K ; and the eddy diffusivity, μ . Analysis of γ_q in the high-resolution simulation gives an average value of 0.1 (not shown) and hence this value is used in 50km_{EECON}. The enstrophy damping parameter, r_Λ , is diagnosed from 5km_{EXP} by taking the volume integral of Equation (14) and

then integrating in time. The damping parameter undergoes an initial adjustment period before reaching a constant value at around 500 days (not shown). Since a constant value of r_Λ is input to the parameterization, the value is taken as that of 5km_{EXP} after the initial adjustment period, which is $5.0 \times 10^{-8} \text{ s}^{-1}$. Since these experiments simulate freely-decaying turbulence and we do not have any damping from bottom friction in the explicit eddy simulations, we set $r_K = 0 \text{ s}^{-1}$. Finally, the diffusivity coefficient, representing the diffusivity of parameterized EKE and eddy potential enstrophy, is set to $\mu = 500 \text{ m}^2 \text{ s}^{-1}$. A minimum value for $|\nabla \bar{q}|$ is specified at each time step to avoid division by zero. A maximum value for κ_{PV} is also specified at each time step.

For the coarse resolution simulation with unconstrained eddy PV fluxes, $50\text{km}_{\text{UNCON}}$, a constant value of κ_{PV} must be specified. We set this to the initial value of κ_{PV} in simulation $50\text{km}_{\text{EECON}}$ which is $100 \text{ m}^2 \text{ s}^{-1}$.

f. Specification of Initial Conditions

Simulations with explicit eddies are initialised with a stream function which is generated at 5km resolution using a similar method as that of the topography. The field generated by the Fourier modes is multiplied by a constant to produce velocities of the order of $1 - 10 \text{ cm s}^{-1}$. This is regridded using volume averaging to 50km resolution for coarse-resolution simulations. The initial stream functions are plotted in figure 3. In configurations with explicit eddies, since there are no forcing terms, it is assumed that the turbulent cascades of energy, and hence the eddies, are driving the large scale flow. Simulations with parameterized eddies are run with no initial stream function and, instead, the parameterized eddies initially drive the flow.

For the coarse resolution simulation with the constrained parameterization, $50\text{km}_{\text{EECON}}$, the initial distributions of K and Λ must be specified. For simplicity, we use constant values K_0 and Λ_0 respectively. We specify K_0 such that the initial parameterized EKE in $50\text{km}_{\text{EECON}}$ is the same as the initial kinetic energy of 5km_{EXP} . We therefore set K_0 to the volume-averaged kinetic energy at time zero in 5km_{EXP} , which is $1.5 \times 10^{-4} \text{ m}^2 \text{ s}^{-2}$. Λ_0 is set to the volume-averaged value of Λ at 500 days in 5km_{EXP} , i.e. after the initial enstrophy adjustment period, which is $1.0 \times 10^{-20} \text{ m}^{-2} \text{ s}^{-2}$.

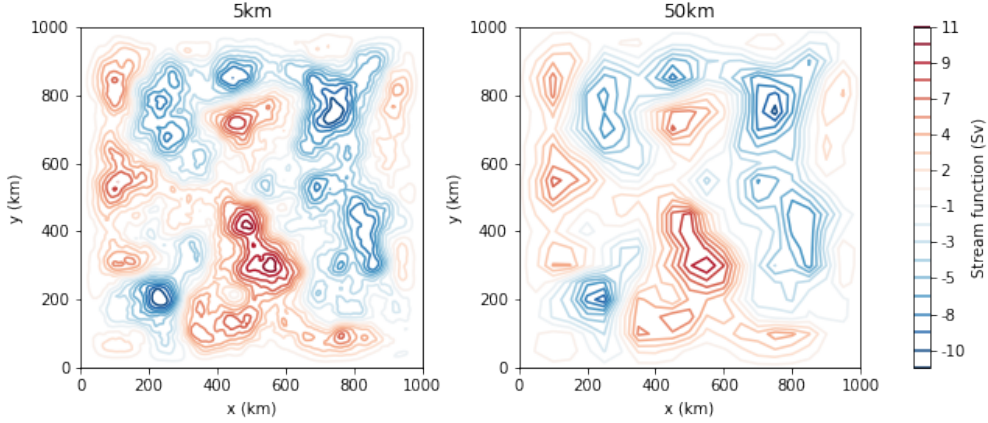


FIG. 3. Initial stream function used in simulations with explicit eddies at 5km resolution (left) and 50km resolution (right).

4. Explicit Eddy Simulations

We compare properties of the mean and eddy flow fields in the eddy-resolving and coarse resolution simulations, 5km_{EXP} and 50km_{EXP} respectively, to identify the unresolved eddy-driven effects on the mean/large-scale flow in the coarse resolution simulation; these effects ideally would be prescribed by the eddy parameterization. Throughout the rest of this paper, the time-mean kinetic energy (MKE), defined as $\bar{\mathbf{u}} \cdot \bar{\mathbf{u}}/2$, is used to represent the large-scale flow for all simulations. The EKE is defined as $\overline{\mathbf{u}' \cdot \mathbf{u}'}/2$ for simulations with explicit eddies. The large-scale potential enstrophy is defined as $\bar{q} \bar{q}/2$ for all simulations, and the eddy potential enstrophy is defined as $\overline{q'q'}/2$ for simulations with explicit eddies. All time-means are taken every 50 days over a 500 day period.

We first identify the effects of the eddies on the energetics which are unresolved in the coarse-resolution simulation and hence need to be parameterized. In 5km_{EXP}, energy is converted from eddy to mean as the simulation progresses, indicated by the simultaneous decrease in EKE and increase in MKE (Figure 4a). In contrast, for 50km_{EXP}, the EKE is damped throughout the simulation but the MKE does not increase and hence there is no conversion of energy from eddy to mean (Figure 4a). This is further illustrated by the eddy to mean energy conversion rate which is positive throughout the majority of the simulation in 5km_{EXP} and zero throughout the

majority of the simulation in 50km_{EXP} (Figure 4b). Hence, we aim to parameterize the effects of this unresolved conversion on the large-scale flow i.e. to parameterize a source of large-scale kinetic energy that mimics the effects of the eddy-to-mean kinetic energy conversion present in the eddy-resolving configuration. Note that the volume averaged kinetic energy of the initial state is of a similar magnitude in both 5km_{EXP} and 50km_{EXP}. However, due to the larger biharmonic diffusion coefficient in 50km_{EXP} than in 5km_{EXP}, the first time-mean value is much smaller in 50km_{EXP} than in 5km_{EXP}.

We now identify the effects of the eddies on the enstrophics which are unresolved in the coarse-resolution simulation and hence need to be parameterized. In both 5km_{EXP} and 50km_{EXP} the eddy potential enstrophy decays with time and there is a large difference in magnitude between the two simulations (Figure 4c). The volume-averaged enstrophy generation term is positive throughout the simulation for 5km_{EXP} (Figure 4d), meaning that the eddy PV fluxes are, on average, fluxing PV down the mean PV gradient for the duration of the simulation. In 50km_{EXP} the enstrophy generation term is much smaller in magnitude than in 5km_{EXP} (Figure 4d) since the eddy field is not well resolved. Hence we require the parameterization to increase the enstrophy generation, thus increasing the magnitude of the eddy potential enstrophy. Note that here and in future sections we do not analyse the mean potential enstrophy since it is dominated by the effects of planetary vorticity and hence the effect of the parameterization on the mean potential enstrophy is negligible.

5. Results of Parameterized Simulations

We now analyse the results of the parameterized simulations, focusing on the four key questions outlined in Section 3.

a. Energy Conversion From Eddy to Mean

The parameterization is able to convert kinetic energy from eddy to mean, shown by the simultaneous decrease in parameterized EKE and increase in MKE in 50km_{EECON} (Figure 5a). This is further confirmed by the parameterized energy conversion term of 50km_{EECON} which is positive throughout the simulation and exhibits similar behaviour in time to that of 5km_{EXP} (Figure 5b).

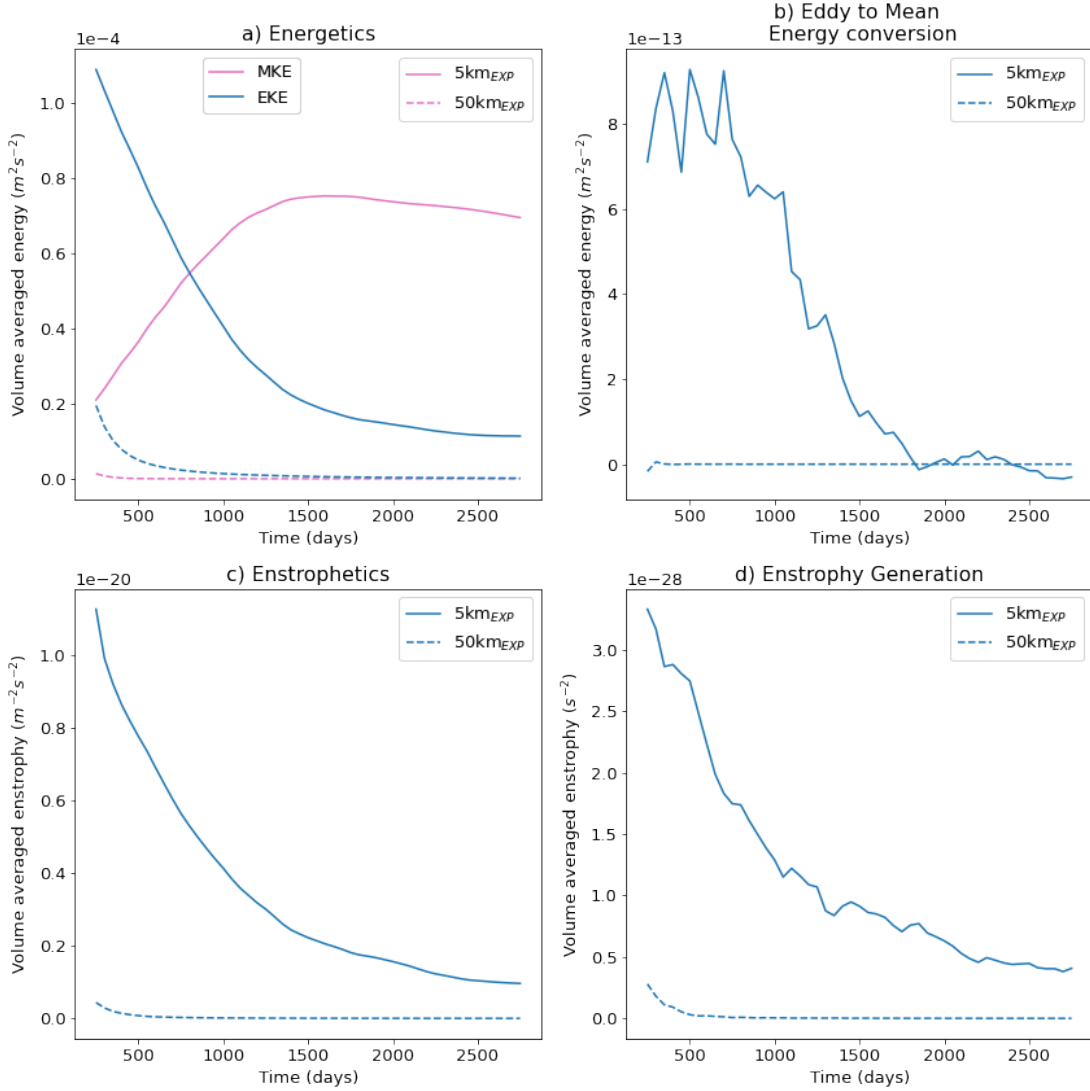


FIG. 4. Data for 5km_{EXP} (solid) and 50km_{EXP} (dashed) showing (a) rolling time-means of MKE (pink) and EKE (blue); (b) the eddy to mean energy conversion term, $-\overline{q'\mathbf{u}'} \cdot \nabla \psi$; (c) eddy potential enstrophy; (d) the enstrophy generation term, $-\overline{q'\mathbf{u}'} \cdot \nabla q$. Rolling time-means are calculated every 50 days over a 500-day period.

The parameterization is able to produce a large-scale topography-following flow as a result of the parameterized eddy-to-mean energy conversion (Figure 6).

b. Energetics and Enstrophetics

We now consider the effects of the parameterization on the energetics and enstrophetics. The peak magnitudes of MKE in 5km_{EXP} and 50km_{EECON} are $7.5 \times 10^{-5} m^2 s^{-2}$ and $3.2 \times 10^{-5} m^2 s^{-2}$

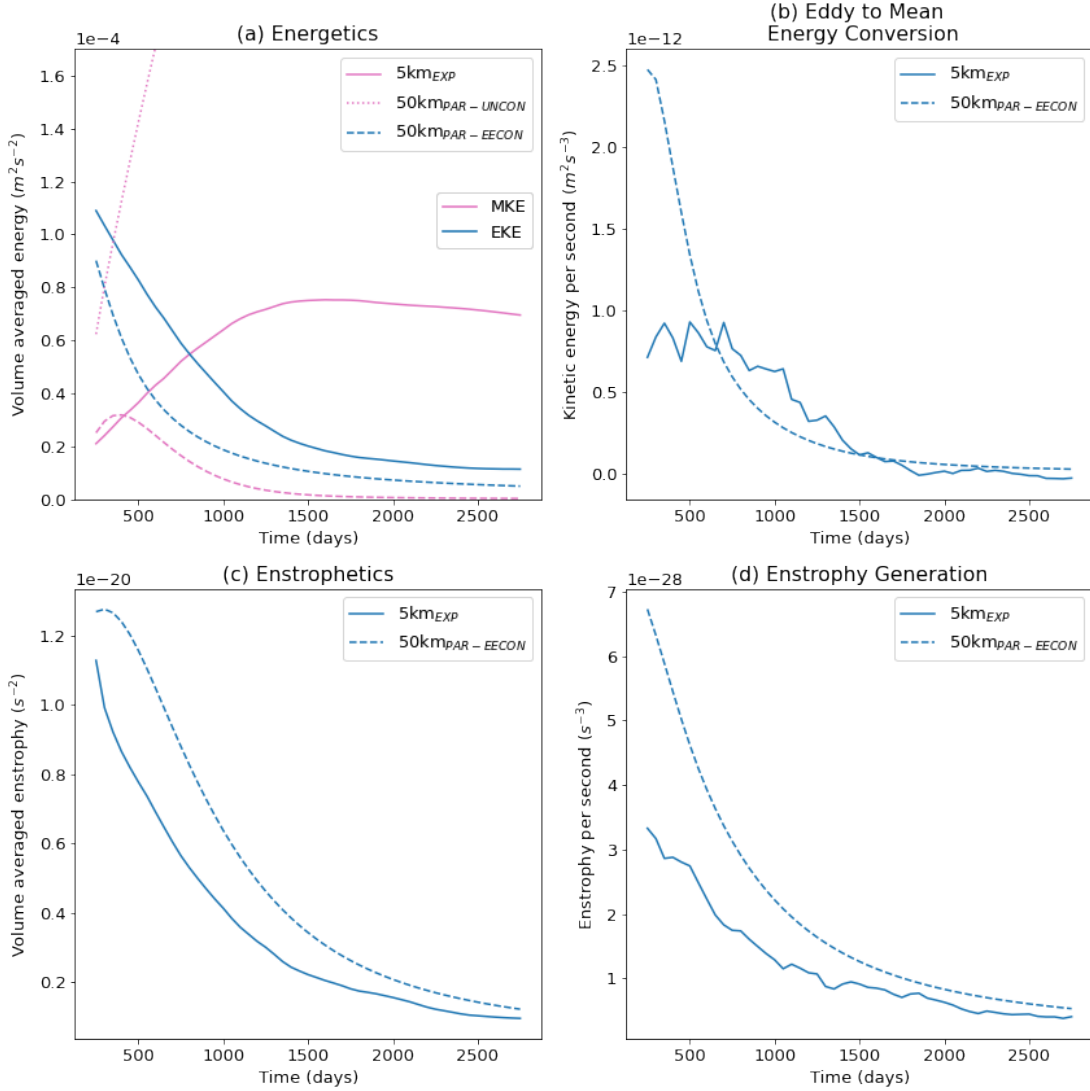


FIG. 5. Data for 5km_{EXP} (solid), 50km_{EECON} (dashed) and 50km_{UNCON} (dotted) showing (a) rolling time-means of MKE (pink) and EKE (blue); (b) the eddy to mean energy conversion term, $-\overline{q'\mathbf{u}'} \cdot \nabla\psi$; (c) eddy potential enstrophy; (d) the enstrophy generation term, $-\overline{q'\mathbf{u}'} \cdot \nabla q$. Rolling time-means are calculated every 50 days over a 500-day period.

respectively. Thus the parameterization leads to a peak MKE of the correct order of magnitude and with a value of 43% of that of the high-resolution simulation. In contrast, the MKE in 50km_{UNCON} increases throughout the simulation, reaching a magnitude almost six times greater than the maximum MKE of 5km_{EXP} by the end of the simulation. The difference in the magnitude of the MKE between 50km_{EECON} and 50km_{UNCON} and the similarity between 50km_{EECON} and

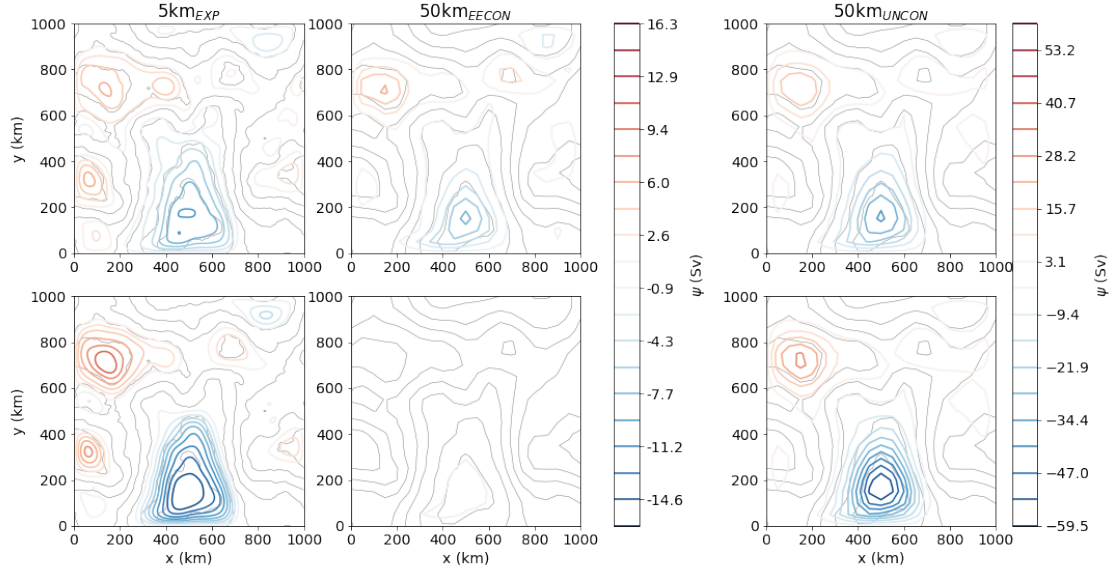


FIG. 6. Time-mean transport stream function for 5km_{EXP} (left), 50km_{EECON} (middle) and 50km_{UNCON} (right) over the time periods 0 - 1500 days (top) and 1501 - 3000 days (bottom). 5km_{EXP} and 50km_{EECON} are plotted on the same colour scale and 50km_{UNCON} is plotted using a separate colour scale for clarity. Grey lines represent topography contours as described in Figure 2.

5km_{EXP} suggests that the kinetic energy of the resolved flow is well-constrained by the energetic and enstrophic constraints imposed. This is further illustrated by the magnitude of the transport stream function (Figure 6) which peaks at a value of 16.3 Sv, 8.3 Sv and 59.5 Sv in 5km_{EXP}, 50km_{EECON} and 50km_{UNCON} respectively. Thus the peak magnitude of the transport stream function is over 250% larger than that of 5km_{EXP} in 50km_{UNCON}, while it is 51% of that of 5km_{EXP} in 50km_{EECON}, further demonstrating that the energetic and enstrophic constraints imposed in 50km_{EECON} are indeed constraining the resolved flow.

The main difference between the energetics of 5km_{EXP} and 50km_{EECON} is the earlier, smaller peak and subsequent decaying of MKE in 50km_{EECON} (Figure 5a). This happens despite the fact that the eddy-to-mean energy conversion in 50km_{EECON} is initially larger in magnitude than that of 5km_{EXP} (Figure 5b). This is due to the difference in biharmonic coefficient between the simulations, which results in a larger damping of resolved kinetic energy in 50km_{EECON} than in 5km_{EXP}.

Both the parameterized eddy potential enstrophy (Figure 5c) and the parameterized enstro-

phy generation (Figure 5d) in $50\text{km}_{\text{EECON}}$ are of the correct order of magnitude and both decay with time in a similar manner to that of their counterparts in 5km_{EXP} . However, both are larger in magnitude than their counterparts in 5km_{EXP} throughout the simulation.

It should be noted that tuning of the input parameters in $50\text{km}_{\text{EECON}}$ might result in an energy conversion and enstrophy generation profile more consistent with that of 5km_{EXP} ; however, here we focus on the functionality of the parameterization, and do not seek to find optimally tuned parameters.

c. Sensitivity of the Output to Input Parameters

We now test the sensitivity of the parameterization to the input parameters (namely r_Λ and γ_q) and the initial conditions (K_0 and Λ_0) by varying these values. We find that the total energy converted from eddy to mean throughout the simulation, total potential enstrophy generated throughout the simulation, and peak MKE value all increase with increasing γ_q and with decreasing r_Λ (Figure 7). An increase in γ_q increases the efficiency of the parameterized eddies to flux PV resulting in a larger eddy PV flux. Decreasing r_Λ increases the parameterized potential enstrophy which also strengthens the eddy PV fluxes. Larger eddy PV fluxes increase PV mixing (since the eddy PV fluxes are down-gradient by design) and therefore increase enstrophy generation. Larger eddy PV fluxes also increase the magnitude of the eddy-to-mean energy conversion, resulting in a larger total amount of energy converted from eddy to mean.

The minimum values of total energy converted and total potential enstrophy generated in this experiment ($8.43 \times 10^{-5} \text{ m}^2\text{s}^{-2}$ and $4.41 \times 10^{-20} \text{ m}^{-1}\text{s}^{-1}$ respectively, Figure 7) are both larger than that of the eddy-resolving simulation ($8.26 \times 10^{-5} \text{ m}^2\text{s}^{-2}$ and $3.23 \times 10^{-20} \text{ m}^{-1}\text{s}^{-1}$ respectively, not shown). Despite this the maximum peak MKE value in this experiment ($4.03 \times 10^{-5} \text{ m}^2\text{s}^{-2}$, Figure 7) is smaller than the peak MKE of the eddy-resolving simulation ($7.53 \times 10^{-5} \text{ m}^2\text{s}^{-2}$, Figure 5a). That is, the parameterized simulations in this experiment all have a higher total energy conversion and total enstrophy generation than that of 5km_{EXP} , but none are able to reach a peak MKE value as high as that of 5km_{EXP} . This is again due to the difference in biharmonic coefficient between the parameterized simulations and the eddy-resolving simu-

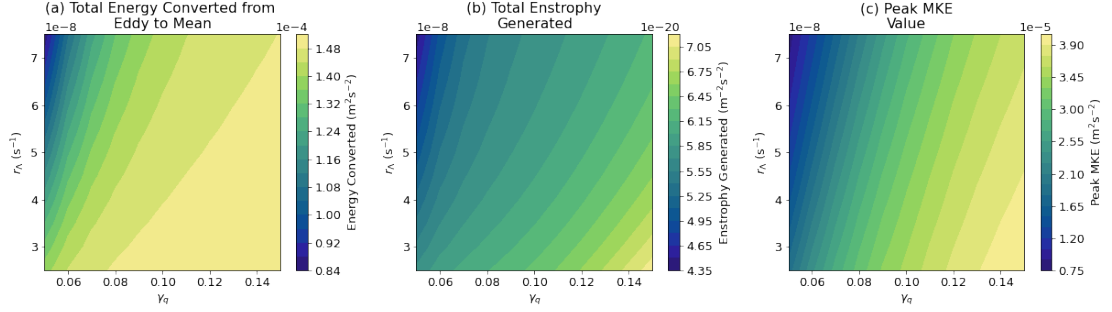


FIG. 7. Contours showing (a) total energy converted from eddy to mean; (b) total enstrophy generated; and (c) peak MKE value for a set of simulations with the same setup as 50km_{EECON} where r_Λ and γ_q are varied by 50% of their value in 50km_{EECON}.

lation, which results in a larger damping of resolved kinetic energy in the parameterized simulations.

A similar experiment is performed varying K_0 and Λ_0 to test the sensitivity of the parameterization to the initial state. We find that the total energy converted from eddy to mean, total enstrophy generated and peak MKE value all increase with increasing K_0 (Figure 8). Increasing K_0 increases the magnitude of the eddy PV fluxes through Equation 9. By a similar argument to that described above, stronger eddy PV fluxes results in an increase in the total enstrophy generated and an increase in the magnitude of the energy conversion. An increase in K_0 also means there is more energy available in the parameterized eddies to be converted. These two things combined result in a larger total amount of energy converted from eddy to mean and hence a larger peak MKE value. In contrast, all three diagnostics show a much smaller sensitivity to Λ_0 than to K_0 , r_Λ or γ_q . This suggests that the strength of the eddy PV fluxes is relatively insensitive to Λ_0 .

6. Summary and Discussion

Traditional methods of parameterizing mesoscale ocean eddies can create spurious sources or sinks of energy when implemented over variable bottom topography and can therefore fail to produce realistic eddy-driven topography-following flows. These flows arise due to the turbulent cascades of kinetic energy and potential enstrophy inherent to quasi-geostrophic flow (Bretherton and Haidvogel 1976). It is therefore sensible to suggest that, in attempting to develop a parameterization for mesoscale eddies which can produce realistic eddy-driven topography-following

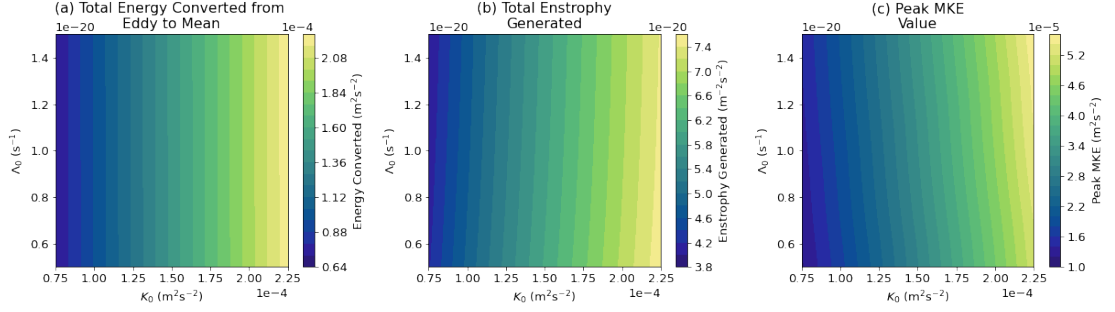


FIG. 8. Contours showing (a) total energy converted from eddy to mean; (b) total enstrophy generated; and (c) peak MKE value for a set of simulations with the same setup as 50km_{EECON} where K_0 and Λ_0 are varied by 50% of their value in 50km_{EECON}.

flows, there should be some consideration of both the kinetic energy and the potential enstrophy. Previous work has seen a number of studies incorporating an energy budget into a mesoscale eddy parameterization (e.g. Cessi (2008); Eden and Greatbatch (2008); Marshall and Adcroft (2010); Marshall et al. (2012)) but, to our knowledge, the same focus has not been applied to the potential enstrophy.

We have presented a new parameterization for barotropic eddies which incorporates an eddy potential enstrophy budget in addition to an eddy kinetic energy budget. The parameterization imposes down-gradient PV mixing in which the strength of the eddy PV fluxes is determined by both the parameterized EKE and eddy potential enstrophy.

The EKE budget employed here includes the following terms: the energy conversion term which accounts for conversion from eddy to mean and vice versa; a dissipation term which represents bottom friction via linear damping; and a redistribution of EKE which we represent as advection by the depth-integrate large-scale flow and Laplacian diffusion. In reality, the redistribution of EKE involves a myriad of processes and our choice of representation may be considered a crude approximation. Nonetheless, we believe this choice to be sufficient as a simple approximation. The eddy potential enstrophy budget includes the following terms: the potential enstrophy generation term which accounts for enstrophy generated through mixing of PV by the parameterized eddies; a dissipation term which represents the viscous dissipation of potential

538 enstrophy at small scales via linear damping; advection by the depth-integrated large-scale flow;
539 and a Laplacian diffusion term. The diffusion terms in both budgets represent the diffusion of each
540 by the eddies and hence they use the same diffusion coefficient. The strength of the parameterized
541 eddy PV fluxes therefore depends on all of these factors. These budgets lead to the following
542 parameters which must be specified: the EKE dissipation parameter, r_K ; the potential enstrophy
543 dissipation parameter, r_Λ ; and the eddy diffusion coefficient, μ . Additionally, the eddy PV flux
544 efficiency parameter, γ_q , must be specified. For simplicity we have chosen to specify a con-
545 stant value for γ_q , despite the fact that in reality γ_q will likely have spatial and temporal dependence.

546
547 The parameterization has been tested in an idealised ocean basin with variable bottom
548 topography, simulating freely-decaying turbulence on an f -plane. Our key findings are:

- 549 1. The parameterization is able to convert kinetic energy from eddy to mean, resulting in a
550 large-scale topography-following flow.
- 551 2. The energetics and enstrophics exhibit similar behaviour to that of an eddy-resolving sim-
552 ulation, with the main difference being an earlier, smaller peak in MKE. This is due to the
553 difference in biharmonic diffusion coefficients in each simulation, which results in a larger
554 damping of resolved kinetic energy in the parameterized simulation. The results suggest the
555 inclusion of the EKE and eddy potential enstrophy budget are sufficient to produce a resolved
556 flow with kinetic energy which is well-constrained, i.e. comparable in magnitude to that of
557 an eddy-resolving simulation.
- 558 3. The input parameters γ_q and r_Λ work as expected with an increase in γ_q and a decrease in r_Λ
559 resulting in a larger eddy-to-mean energy conversion. The resolved flow depends on K_0 , the
560 EKE of the initial state, with a larger K_0 resulting in a larger eddy-to-mean energy conversion.
561 The resolved flow is relatively insensitive to Λ_0 , the eddy potential enstrophy of the initial
562 state.

563 The parameterization provides a mechanism through which energy can be transferred from
564 unresolved to resolved scales and hence can backscatter energy. Currently, the source of the
565 unresolved kinetic energy is the EKE of the initial state, whilst in other energy backscatter
566 parameterizations it is the kinetic energy dampened at the grid scale via explicit viscosity (e.g.

567 Jansen and Held (2014); Mana and Zanna (2014)). The use of an EKE budget in the framework
568 outlined here opens up the possibility of introducing other sources of EKE, which could be
569 explored in future work.

570

571 There are some significant limitations to the parameterization as it is in its current form.
572 Firstly, it is a known problem that, in a multiply-connected domain, integral constraints on the eddy
573 PV fluxes must be satisfied in order for angular momentum conservation to hold (Marshall 1981).
574 The current form of the parameterization does not satisfy this constraint and hence further work is
575 required to employ the parameterization in multiply-connected domains, e.g. with a circumpolar
576 Southern Ocean. Additionally, we have specified that the eddy PV fluxes are directed down the
577 mean PV gradient, which is true on average but may not hold locally. For example, up-gradient
578 eddy PV fluxes are important in driving time-mean recirculation gyres in a wind-driven setup
579 (Waterman and Hoskins 2013). Hence, there are important instances where the parameterization
580 in its current form is not able to capture the full effect of the eddies on the mean flow.

581

582 There are further questions which remain to be addressed. We have shown that the pa-
583 rameterization can convert energy from eddy to mean, but it remains to be determined if it can
584 also convert energy from mean to eddy in a sensible manner. Future work could determine this
585 by testing the parameterization in a wind-driven gyre, in which the mean-to-eddy conversion
586 is crucial in modulating the strength of the wind-driven jet (Waterman and Hoskins 2013). As
587 mentioned previously, it is highly likely that the results of the parameterization depend on the
588 representation of the terms in the energy and enstrophy budgets which we have not investigated
589 here. Testing the parameterization with different iterations of energy and enstrophy budget may be
590 useful in determining the effect of each on the resolved flow. Additionally, for simplicity, we have
591 chosen to specify constant values for the parameters associated with the parameterization, but they
592 will likely be variable in both space and time. We have not attempted to define the optimal choice
593 of input parameters, nor have we specified what to optimize towards, since we have tested the
594 parameterization in a highly idealised setup. Understanding of the key controls on the space-time
595 variability of these parameters will be crucial in determining the optimal parameter set-up for a
596 more realistic configuration.

597

598 Finally, we have so far implemented and tested the parameterization in a barotropic setup.
599 How the parameterization should be implemented in a baroclinic setup remains to be determined.
600 Future work could explore the extent to which the new parameterization can be included, alongside
601 GM90, to represent the rectified forcing of the large-scale flow along topography contours by
602 barotropic eddies.

603 *Acknowledgments.* Financial support was provided by the UK Natural Environment Research
604 Council (NE/S007474/1) and the Oxford-Radciffe Scholarship. Collaboration was made possible
605 by funding from University College Oxford and the Mitacs Globalink Research Award. Stephanie
606 Waterman acknowledges funding from the Natural Sciences and Engineering Research Council
607 of Canada (NSERC) Discovery Grants Program (NSERC-2020-05799). This work utilised the
608 ARCHER2 UK National Supercomputing Service (<https://www.archer2.ac.uk/>).

609 *Data availability statement.* The code used for experiments discussed in this work can be found
610 at https://github.com/rosieeaves/barotropic_model. Questions with regards to this code should be
611 directed to Rosie Eaves.

612 **References**

613 Adcock, S. T., and D. P. Marshall, 2000: Interactions between geostrophic eddies and the mean
614 circulation over large-scale bottom topography. *J. Phys. Oceanogr.*, **30**, 3223–3238.

615 Arakawa, A., 1966: Computational design for long term numerical integration of the equations of
616 fluid motion: two-dimensional incompressible flow. part i. *J. Comput. Phys.*, **1**, 119–143.

617 Arnold, V. I., 1965: Conditions for nonlinear stability of stationary plane curvilinear flows of an
618 ideal fluid. *Dokl. Akad. Nauk. SSSR.*, **162**, 975–978.

619 Bachman, S. D., 2019: The gm+e closure: A framework for coupling backscatter with the gent and
620 mcwilliams parameterization. *Ocean Modell.*, **136**, 85–106, <https://doi.org/10.1016/j.ocemod.2019.02.006>.

622 Bretherton, F. P., and D. B. Haidvogel, 1976: Two-dimensional turbulence above topography. *J.*
623 *Fluid Mech.*, **78** (1), 129–154, <https://doi.org/10.1017/S002211207600236X>.

624 Cessi, P., 2008: An energy-constrained parameterization of eddy buoyancy flux. *J. Phys. Oceanogr.*,
625 **38**, 1807–1819, <https://doi.org/10.1175/2007JPO3812.1>.

626 Danabasoglu, G., J. C. McWilliams, and P. R. Gent, 1994: The role of mesoscale tracer transports
627 in the global ocean circulation. *Science*, **264**, 1123–1126.

628 Eby, M., and G. Holloway, 1994: Sensitivity of a large-scale ocean model to a parameterization of
629 topographic stress. *J. Phys. Oceanogr.*, **24**, 2577–2588.

630 Eden, C., and R. J. Greatbatch, 2008: Towards a mesoscale eddy closure. *Ocean Modell.*, **20**,
631 223–239, <https://doi.org/10.1016/j.ocemod.2007.09.002>.

632 Eyring, V., S. Bony, G. A. Meehl, C. A. Senior, B. Stevens, R. J. Stouffer, and K. E. Taylor, 2016:
633 Overview of the coupled model intercomparison project phase 6 (cmip6) experimental design and
634 organization. *Geosci. Model Dev.*, **9**, 1937–1958, <https://doi.org/10.5194/gmd-9-1937-2016>.

635 Gent, P. R., and J. C. McWilliams, 1990: Isopycnal mixing in ocean circulation models. *J. Phys.*
636 *Oceanogr.*, **20**, 150–155.

637 Green, J. S. A., 1970: Transfer properties of the large-scale eddies and the general circulation of
638 the atmosphere. *Q. J. R. Meteorol. Soc.*, **96**, 157–185, <https://doi.org/10.1002/qj.49709640802>.

639 Gregory, J. M., and Coauthors, 2016: The flux-anomaly-forced model intercomparison project
640 (fafmip) contribution to cmip6: Investigation of sea-level and ocean climate change in response
641 to co2 forcing. *Geosci. Model Dev.*, **9**, 3993–4017, <https://doi.org/10.5194/gmd-9-3993-2016>.

642 Griffies, S. M., and Coauthors, 2009: Coordinated ocean-ice reference experiments (cores). *Ocean*
643 *Modell.*, **26**, 1–46, <https://doi.org/10.1016/j.ocemod.2008.08.007>.

644 Griffies, S. M., and Coauthors, 2016: Omip contribution to cmip6: experimental and diagnostic
645 protocol for the physical component of the ocean model intercomparison project. *Geosci. Model*
646 *Dev.*, **9**, 3231–3296, <https://doi.org/10.5194/gmd-9-3231-2016>.

647 Holloway, G., 1992: Representing topographic stress for large-scale ocean models. *J. Phys.*
648 *Oceanogr.*, **22** (9), 1033–1046, [https://doi.org/10.1175/1520-0485\(1992\)022<1033:RTSFLS>](https://doi.org/10.1175/1520-0485(1992)022<1033:RTSFLS>2.0.CO;2)
649 2.0.CO;2.

650 Jansen, M. F., and I. M. Held, 2014: Parameterizing sub-grid scale eddy effects using energetically
651 consistent backscatter. *Ocean Modell.*, **80**, 36–48, [https://doi.org/10.1016/j.ocemod.2014.06.](https://doi.org/10.1016/j.ocemod.2014.06.002)
652 002.

653 Jones, C. D., and Coauthors, 2016: C4mip-the coupled climate-carbon cycle model intercompari-
654 son project: Experimental protocol for cmip6. *Geosci. Model Dev.*, **9**, 2853–2880, [https://doi.org/](https://doi.org/10.5194/gmd-9-2853-2016)
655 10.5194/gmd-9-2853-2016.

- 656 Mana, P. P., and L. Zanna, 2014: Toward a stochastic parameterization of ocean mesoscale eddies.
657 *Ocean Modell.*, **79**, 1–20, <https://doi.org/10.1016/j.ocemod.2014.04.002>.
- 658 Marshall, D. P., and A. J. Adcroft, 2010: Parameterization of ocean eddies: Potential vorticity mix-
659 ing, energetics and arnold’s first stability theorem. *Ocean Modell.*, **32**, 188–204, [https://doi.org/](https://doi.org/10.1016/j.ocemod.2010.02.001)
660 [10.1016/j.ocemod.2010.02.001](https://doi.org/10.1016/j.ocemod.2010.02.001).
- 661 Marshall, D. P., J. R. Maddison, and P. S. Berloff, 2012: A framework for parameterizing eddy po-
662 tential vorticity fluxes. *J. Phys. Oceanogr.*, **42**, 539–557, [https://doi.org/10.1175/JPO-D-11-048.](https://doi.org/10.1175/JPO-D-11-048.1)
663 [1](https://doi.org/10.1175/JPO-D-11-048.1).
- 664 Marshall, D. P., R. G. Williams, and M.-M. Lee, 1999: The relation between eddy induced
665 transport and isopycnic gradients of potential vorticity. *J. Phys. Oceanogr.*, **29**, 1571–1578,
666 [https://doi.org/10.1175/1520-0485\(1999\)029<1571:TRBEIT>2.0.CO;2](https://doi.org/10.1175/1520-0485(1999)029<1571:TRBEIT>2.0.CO;2).
- 667 Marshall, J. C., 1981: On the parameterization of geostrophic eddies in the ocean. *J. Phys.*
668 *Oceanogr.*, **11**, 257–271.
- 669 Nazarenko, L., G. Holloway, and N. Tausnev, 1998: Dynamics of transport of ”atlantic signature” in
670 the arctic ocean. *J. Geophys. Res.*, **103**, 31 003–31 015, <https://doi.org/10.1029/1998JC900017>.
- 671 N, O. A., and P. E. Isachsen, 2003: The large-scale time-mean ocean circulation in the nordic seas
672 and arctic ocean estimated from simplified dynamics. *J. Mar. Res.*, **61**, 175–210.
- 673 Rhines, P. B., 1975: Waves and turbulence on a beta-plane. *J. Fluid Mech.*, **69**, 417–443,
674 <https://doi.org/10.1017/S0022112075001504>.
- 675 Tamarin, T., J. R. Maddison, E. Heifetz, and D. P. Marshall, 2016: A geometric interpreta-
676 tion of eddy reynolds stresses in barotropic ocean jets. *J. Phys. Oceanogr.*, **46**, 2285–2307,
677 <https://doi.org/10.1175/JPO-D-15-0139.1>.
- 678 Wang, H., S. Legg, and R. Hallberg, 2018: The effect of arctic freshwater pathways on north
679 atlantic convection and the atlantic meridional overturning circulation. *J. Climate*, **31**, 5165–
680 5188, <https://doi.org/10.1175/JCLI-D-17-0629.1>.

681 Waterman, S., and B. J. Hoskins, 2013: Eddy shape, orientation, propagation, and mean flow
682 feedback in western boundary current jets. *J. Phys. Oceanogr.*, **43**, 1666–1690, [https://doi.org/](https://doi.org/10.1175/JPO-D-12-0152.1)
683 10.1175/JPO-D-12-0152.1.

684 Zanna, L., P. P. Mana, J. Anstey, T. David, and T. Bolton, 2017: Scale-aware deterministic
685 and stochastic parameterizations of eddy-mean flow interactions. *Ocean Modell.*, **111**, 66–80,
686 <https://doi.org/10.1016/j.ocemod.2017.01.004>.